

Synthesis and characterization of Y^{3+} -doped TiO_2 nanocomposites for photocatalytic applications

Himanshu Narayan¹, Hailemichael Alemu², Lebohang Macheli²,
Madhavi Thakurdesai³ and T K Gundu Rao⁴

¹ Department of Physics and Electronics, National University of Lesotho, Roma 180, Lesotho, Southern Africa

² Department of Chemistry and Chemical Technology, National University of Lesotho, Roma 180, Lesotho, Southern Africa

³ Department of Physics, Birla College, Kalyan 421304, India

⁴ SAIF, Indian Institute of Technology, Powai, Mumbai 400076, India

E-mail: h.narayan@nul.ls and hm.alemu@nul.ls

Received 16 March 2009, in final form 27 April 2009

Published 3 June 2009

Online at stacks.iop.org/Nano/20/255601

Abstract

The $TiO_2 \cdot [Y_2O_3]_x$ ($x = 0.1-0.4$) nanocomposites (NCs) with an average particle size of 74 nm were prepared by the method of chemical co-precipitation followed by hydrolysis (CPH). Their visible light photocatalytic activity was investigated for the degradation of congo red (CR) dye. All NCs showed improved degradation as compared to the polycrystalline samples of similar compositions prepared by the solid-state reaction (SSR) route (average particle size of a few micrometers), as well as to the pure TiO_2 . The better photocatalytic activity of the NCs was attributed to their smaller particle size. Another comparison of the results with those obtained with Zn^{2+}/Fe^{3+} ions co-doped TiO_2 NCs, under similar experimental conditions, revealed that in the Y^{3+} -doped NCs, particle size might not be the only factor responsible for the improved photocatalytic properties. It was concluded that the Y^{3+} ion-mediated suppression of the unwanted e^-/h^+ recombination could be the possible factor leading to additional enhancement.

(Some figures in this article are in colour only in the electronic version)

1. Introduction

Titanium oxide (TiO_2) is a wide bandgap (3.2 eV) semiconductor with a number of interesting electronic and optical properties. Currently, a lot of work on this material is being carried out by several groups all over the world. Degradation of pollutants by photocatalysis, which is a well-known process employed for the treatment of wastewater, is one of the most remarkable applications of titanium oxide [1, 2]. With several possibilities to improve the photocatalytic properties of pure TiO_2 , great efforts are being made by chemists and material scientists. However, to find any viable technique, it is important to understand the mechanisms involved in the TiO_2 mediated photocatalysis.

There are two widely accepted mechanisms [3, 4] to explain the photocatalytic oxidation process mediated by a semiconductor.

- (i) Photo-excitation: electrons can be excited by irradiation with suitable wavelengths from the valence band (VB) of the semiconductor to its conduction band (CB). The excited electrons, as well as the holes left behind in the VB of the material, can react with oxygen, water and hydroxide ions to form highly active oxygen species. These active species can then react with the pollutants leading to their degradation. In this process obviously the bandgap of the semiconductor plays a major role.
- (ii) Photosensitization: pollutants (e.g. dyes) after getting adsorbed on the surface of the catalyst (semiconductor) particles, start absorbing visible radiations. In the process they get photochemically excited and transfer an electron to the particle. This transfer produces a superoxide anion radical from reduction of the molecular oxygen, and at the same time a cation radical is produced from the pollutant, which may lead to the degradation of other pollutant

molecules. Clearly, this mechanism should depend on the effective surface area of the catalyst.

Obviously, therefore, the photocatalytic yield of TiO₂ can be improved by: (i) narrowing the bandgap, so that visible light-induced photocatalysis is made possible and (ii) reducing the particle size so as to increase the specific surface area. The 3.2 eV bandgap of pure TiO₂ corresponds to a band edge (or cutoff wavelength, λ_{cutoff}) of about 390 nm, which falls inside the UV region of the spectrum. So, the wavelengths larger than this value are not used in the excitation of VB electrons, and consequently visible light photocatalysis by photo-excitation is not possible. However, the pure material can be modified, for example by suitable doping, so as to narrow the bandgap in such a way that visible light is efficiently utilized in photocatalysis. In this direction, several authors have reported doping of TiO₂ with narrower band-gap semiconductors, such as CdS [5], CdSe [6], FeS₂ [7], RuS₂ [8], WO₃ [9, 10], ZnFe₂O₄ [11–13], etc. Additionally, by employing an appropriate method of synthesis, particles with reduced size can be obtained, and thus the specific surface area of TiO₂ can be increased in order to facilitate additional photosensitization. Studies along this line, e.g. with the nanostructures of pure TiO₂ [3, 14–16], as well as with nanomaterials based on TiO₂ [12, 17, 18] are also well documented.

Apart from these two important aspects, the recombination of photo-generated electrons with holes (e^-/h^+ recombination), which severely hampers the photocatalytic activity of the material, also needs to be taken into account. Several methods have been suggested by various groups. For example, doping of some transition metal ions (e.g. Fe³⁺, Cu²⁺, Mn²⁺, etc) can enhance the photocatalytic activity, either by trapping photo-generated electrons in TiO₂ [19], or due to the formation of reactive complexes [20, 21].

However, it is important to note that, although having smaller particles can help to improve the photocatalytic activity, it may not always be conducive to the other two requirements. This is because, for very small particles (size <10 nm), generally the bandgap could be wider than that of the bulk owing to the quantum size effect [22]. As a result, the λ_{cutoff} could blueshift, leading to shifting the useful regions of the spectrum more towards smaller wavelengths, instead of the required shift towards visible regions. Similarly, the e^-/h^+ recombination could also become significantly higher at smaller dimensions [14], which could result in further reduction of the photocatalytic activity. In order to achieve optimum efficiency, therefore, one needs to strike a balance between all three of these decisive factors.

Recently, we have reported that modification of the bandgap may not be entirely responsible for better visible light photocatalysis in some TiO₂ based nanocomposites [13]. Contrary to what was reported earlier by some of the authors [11], we have argued that ZnFe₂O₄ doping only plays a limited role, probably in controlling the e^-/h^+ recombination only. Even if the bandgap is not narrowed by doping, the visible light photocatalysis can still progress by photosensitization and can still be improved, for example, by increasing the effective surface area. In order to consolidate

our assertion further, we are reporting in this paper, for the first time, about the visible light photocatalytic degradation of the dye congo red (CR) using Y₂O₃ (Y³⁺ ions)-doped TiO₂ nanocomposites.

Based on the recent results of our investigation, we presume that for nanosized TiO₂ mediated photocatalysis, bandgap modification is perhaps the least important of the three decisive factors mentioned above. Therefore, in the present work, we attempt to investigate the significance of the other two factors, i.e. particle size and e^-/h^+ recombination. We have selected Y₂O₃ as the dopant because of its bandgap of about 4.5 eV ($\lambda_{\text{cutoff}} = 275$ nm) [23], which is wider than that of pure TiO₂. The resultant composites, therefore, are not at all expected to absorb in the visible regions of the spectrum. Thus, the possibility of visible light photocatalysis by photo-excitation can be thoroughly ruled out and consequently the effects of photosensitization can be investigated exclusively. Moreover, since the rare earth ions are known for efficiently trapping electrons, Y³⁺ doping is also expected to enhance photocatalytic activity by suppressing the undesired e^-/h^+ recombination [24–26].

2. Experimental details

2.1. Material synthesis

The TiO₂·[Y₂O₃]_x NCs with $x = 0.1$ – 0.4 were prepared by the method of chemical co-precipitation followed by hydrolysis (CPH), as reported in the literature for TiO₂·[ZnFe₂O₄]_x materials [11, 13]. Chemicals used in the synthesis were yttrium (III) nitrate hydrate Y(NO₃)₃·6H₂O (Riedel-de Haën), n-propanol (BDH), iso-propanol (UNILAB, SA), tetrabutyl-orthotitanate (Fluka) and nitric acid (ACE, SA). The CR used in these experiments was obtained from Aldrich Chemical Co. First, the Y₂O₃ was precipitated from Y(NO₃)₃·6H₂O solution which was prepared by dissolving the nitrate in isopropyl alcohol and heating the mixture for 30 min at 65 °C with continuous stirring. The pH of the solution was raised to 6.5 by slowly adding a 3.5 M NH₄OH solution in isopropyl alcohol, to precipitate the nitrate precursor. Then approximately 10 g of distilled and deionized water was added dropwise to the solution and was stirred for 45 min. A solution of tetrabutyl-orthotitanate (Ti(OBu)₄) and isopropyl alcohol was prepared in a ratio of 1:2 by weight and added dropwise to the co-precipitated Y₂O₃ solution for controlled hydrolysis with H₂O:Ti(OBu)₄ in the ratio of 25:1. The final solution was kept stirred for 90 min at 65 °C, filtered, and then dried at 100 and 220 °C, respectively. The prepared TiO₂·[Y₂O₃]_x nanoparticles were then calcined in a flowing air atmosphere at 500 °C for 3 h.

Polycrystalline composite samples of TiO₂·[Y₂O₃]_x (with $x = 0.1$ – 0.4) were also prepared by the solid-state reaction (SSR) route. The Y₂O₃ used in the preparation was freshly prepared by heating the nitrate at 450 °C for about 1 h. Stoichiometric amounts of highly pure (99.9%) TiO₂ and Y₂O₃ were taken in an agate mortar with some ethanol and thoroughly ground for about 1 h. The resultant mixtures were then allowed to dry for about 1 h at 60 °C. This was followed by calcination of the samples at 600 °C for 2 h.

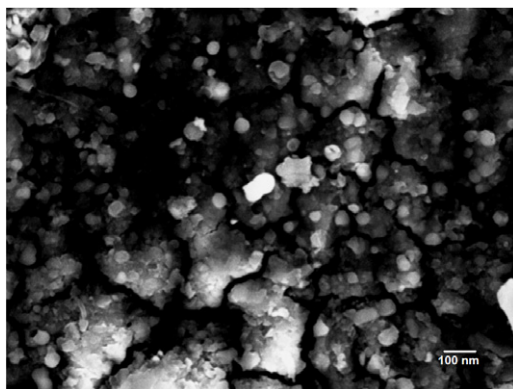


Figure 1. Typical SEM picture of chemically synthesized $\text{TiO}_2\cdot[\text{Y}_2\text{O}_3]_x$ nanocomposite (for $x = 0.1$ composition).

2.2. Measurements

Characterization of all the samples was done using scanning electron microscopy (SEM), powder x-ray diffraction (XRD), particle size analyzer and Raman spectroscopy. The SEM was taken on a JEOL JSM5600 scanning electron microscope from JEOL, Japan. The XRD of the powdered samples was carried out on a Shimadzu D6000 diffractometer (Shimadzu, Japan) using $\text{Cu K}\alpha$ radiation ($\lambda = 1.5406 \text{ \AA}$). The particle size was measured using a Microtrac/Nanotrac TM150 particle size analyzer, which employs optical light scattering measurements of composite particles in a water suspension. Raman spectra were recorded with the 514 nm green excitation light (laser output: 20 mW) using a LabRAM HR machine from Jobin Yvon.

After characterization, the visible light photoactivity of all the samples, the NCs (CPH synthesized) as well as the polycrystalline materials (SSR prepared), in the degradation of the dye CR was carried out in a locally fabricated photoreactor. Details about the construction and functioning of the photoreactor are reported elsewhere [13]. Prior to the photocatalysis experiments, the optimum concentrations of CR and TiO_2 for the best possible degradation results were determined. It was noted that the rate of degradation depends on the amount of the catalyst as well as on that of the dye. When all the dye is adsorbed on TiO_2 , further addition of catalyst decreases the rate because of the increased opacity of the solution. Also, since the amount of the absorbed radiation depends on the concentration of the dye, there exists a certain concentration for which the light absorption is maximum. Based on the results of optimization, a solution with 25 mg of CR per liter of water was prepared and 850 ml of this experimental solution, 275 mg of photocatalyst sample and a stirring bar were placed in the photoreactor and the fluorescent lamp was turned on to start the photoreaction. The solution was stirred throughout the duration of the experiment. At predetermined durations of time, 1.5 ml of the solution was taken out from the photoreactor and centrifuged. Absorbance of the resulting clear solution was measured at 498 nm excitation wavelength, using a UV-vis Shimadzu model 1201 spectrophotometer. To see the dependence of degradation on the presence of catalyst and light alone, the absorbance of

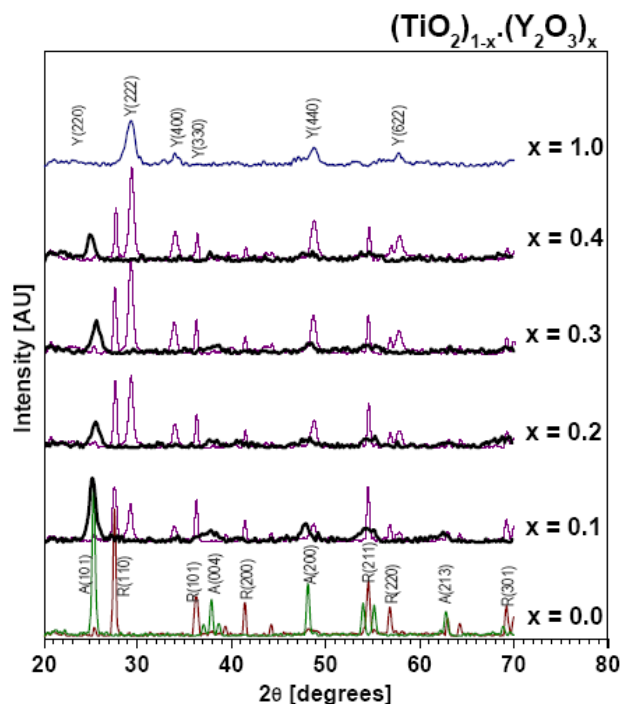


Figure 2. X-ray diffraction patterns for various compositions ($x = 0.1-0.4$) of the $\text{TiO}_2\cdot[\text{Y}_2\text{O}_3]_x$ samples prepared by chemical synthesis (thick lines) and by the solid-state reaction method (thin lines). The patterns for pure TiO_2 ($x = 0.0$) and pure Y_2O_3 ($x = 1$) are also shown. The peaks corresponding to the various reflections of the constituent oxides are shown by the letters R (rutile TiO_2), A (anatase TiO_2) and Y (Y_2O_3).

solutions with photocatalyst samples but in the absence of light, and in light but without any sample, were also measured.

3. Results and discussion

The SEM pictures of chemically synthesized $\text{TiO}_2\cdot[\text{Y}_2\text{O}_3]_x$ NCs show grains of approximately 70–80 nm size. A typical SEM picture is depicted in figure 1.

3.1. X-ray diffraction

X-ray diffraction (XRD) patterns for the various composite samples prepared by CPH synthesis are shown in figure 2. For a comparison and identification of the peaks, the XRD patterns of similar compositions of samples prepared by the SSR process (which as expected produces more crystalline composites) have also been plotted using the same scales. Moreover, the figure also shows the patterns obtained for the pure oxides, i.e. both rutile and anatase phases of TiO_2 powder, as well as the Y_2O_3 powder.

Sharp peaks corresponding to the samples prepared by the SSR method indicate the more crystalline nature of the powder and thus facilitate the identification of various phases of precursor powders in the composites. Apparently, the main constituent of these composites is the rutile phase of TiO_2 . With the increasing value of molar concentration x in the composites, a gradually decreasing amount of TiO_2 is revealed

by the decreasing heights of the $2\theta = 27.4^\circ$ (110), 36.1° (101), 39.2° (200), 54.3° (211), 56.6° (220) and 69.0° (301) rutile peaks. On the other hand, the gradual increase of Y_2O_3 with x in the SSR-prepared composites is indicated by the increasing heights of the $2\theta = 29.22^\circ$ (222), 33.8° (400), 48.6° (440) and 57.7° (622) peaks of the oxide.

In the XRD patterns for the NCs prepared by CPH, the broadened (larger FWHM as compared to those prepared by SSR) peaks directly indicate the formation of particles with reduced size. The crystallite size calculated from the XRD data, as discussed in the next section, confirms that CPH has indeed produced nanosized particles (or nanocomposites), although these NC samples are primarily anatase. In all the composites prepared by CPH, the most prominent peak at $2\theta = 25.7^\circ$ corresponds to the (101) peak of the anatase TiO_2 phase. The presence of the (200) anatase peak at $2\theta = 48.8^\circ$ is also significant, although it appears as a spread which is apparently a combination of this peak and the (440) Y_2O_3 peak at $2\theta = 48.6^\circ$. Other anatase peaks (e.g. $2\theta = 37.5^\circ$ (103), 38.4° (004), 39.2° (112), 54.8° (105), 54.9° (121)(211) and 63.1° (213)(123)) appear mostly as spreads with very small heights at the scale used in the plots.

3.2. Particle size analysis

The crystallite (defined as the smallest possible regions of the sample that reflect the incident x-rays coherently) size z of each sample was estimated using the Scherrer formula [27] from the FWHM of the Gaussian best-fit to the prominent peaks in the XRD data. It was found that values of z for the rutile and anatase TiO_2 powders were around 52 and 57 nm, respectively, whereas for the Y_2O_3 , it was about 17 nm. For the composites, an average crystallite size of around 41 nm was estimated for samples prepared through the SSR route, and for those prepared by the CPH route the average crystallite size was determined to be 17 nm.

The grain size of all the samples was also determined by the particle size analyzer, which measures the average diameter of the grains. The results obtained from these measurements are shown in figure 3 as the distribution of the number of particles with size. For the starting materials used in the solid-state reaction process, the average grain size was found to be 2.4 and 3.0 μm for TiO_2 and Y_2O_3 powders, respectively. An average grain size of more than 1 μm was found for the samples prepared by the SSR route (from about 3.3 μm for $x = 0.1$ to about 2.1 μm for $x = 0.4$), which decreased with the addition of Y_2O_3 , probably because of the comparatively smaller particle size of the latter. On the other hand, the average grain size for the CPH samples was found to be about 74 nm, which was almost uniform for all the compositions.

At this point, it is noteworthy to mention that the measurement of crystallite size from the XRD data using the Scherrer formula has its own limitations. Nevertheless, it serves the purpose of materials scientists working with nanoparticles in the sense that it immediately gives a rough estimation of the size without much effort [28]. Moreover, it is also important to understand that the 'crystallite size' is completely different from the 'grain' or the 'particle size' that

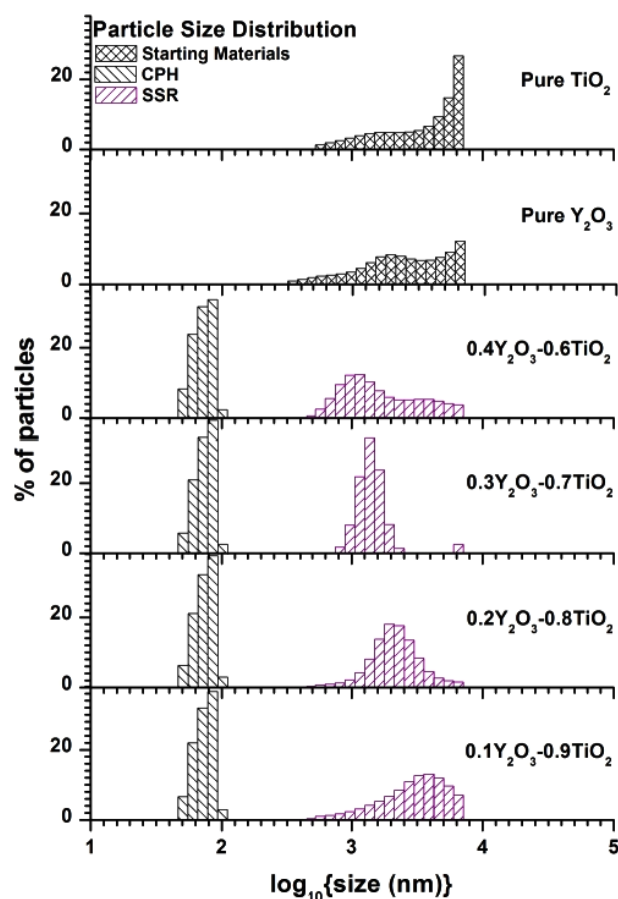


Figure 3. Particle size distribution for various compositions of the $TiO_2 \cdot [Y_2O_3]_x$ samples with $x = 0.0-0.4$ prepared by two different methods. The size distributions of pure TiO_2 and Y_2O_3 are also shown.

may be observed under the microscope, e.g. the SEM. Since the x-rays can penetrate through the surface of the particles, what is measured through XRD is actually the size of the small domains (the so-called 'crystallites') within the grains that diffract the x-rays coherently [29]. Thus, one grain could be made up of several crystallites, depending upon the method of preparation. In the present case, a comparison of the crystallite size (from XRD data) with the grain size (measured from MicroTrac size analyzer) seems to reveal that a single grain of the samples prepared by SSR could consist of several thousand crystallites, whereas that of those synthesized by CPH is made up of about 10–15 crystallites only. This difference may be attributed obviously to the longer time available in the SSR process for agglomeration of the crystallites into grains.

3.3. Raman spectroscopy

Figure 4 shows the Raman spectra for various compositions of the CPH-synthesized $TiO_2 \cdot [Y_2O_3]_x$ NCs. Qualitatively, the Raman profiles obtained for our samples indicate the presence of the anatase phase as the main constituent in all the NCs, which is in agreement with the XRD results. The five distinct anatase peaks at 151, 196, 409, 515 and 633 cm^{-1} , which are assigned to the E_g , E_g , B_{1g} , A_{1g} or

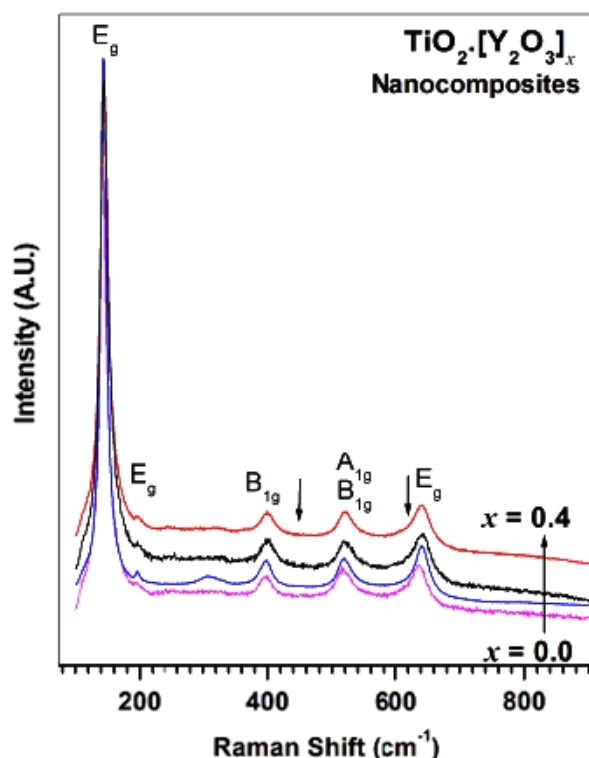


Figure 4. Raman spectra of $\text{TiO}_2 \cdot [\text{Y}_2\text{O}_3]_x$ nanocomposites powders prepared by chemical synthesis showing the Raman modes for anatase phase. Arrows indicate the expected positions of rutile peaks.

B_{1g} and E_g modes, respectively [30, 31], are clearly visible. However, the peaks corresponding to the 151 and 409 cm^{-1} are slightly redshifted to around 141 and 398 cm^{-1} , respectively. Zhang *et al* [30] have correlated the occurrence of such shifts with the crystallite size (estimated from XRD data) of the samples, in the framework of a phonon confinement model. They have reported that, as the crystallite size decreases, the lowest frequency E_g mode peak blueshifts gradually, and for a crystallite size of about 28 nm, the latter peaks around 145 cm^{-1} . From the XRD data, the average crystallite size of the NCs was found to be about 17 nm, which satisfactorily explains the redshifts of the E_g mode peak observed in our measurements. It is noteworthy here that in $\text{TiO}_2 \cdot [\text{ZnFe}_2\text{O}_4]_x$ NCs with an average crystallite size of about 29 nm, we have found that the E_g mode peaks around 145 cm^{-1} , which is also in line with the present observations [13]. The absence of a rutile phase (Raman peaks around 450 and 610 cm^{-1}) in the CPH-synthesized samples, as observed in the XRD, is also supported by the Raman spectroscopy results.

3.4. Photocatalytic activity

The visible light ($\lambda > 420$ nm) photocatalytic activity of all the composites was examined for the degradation of the dye CR. Per cent degradation in terms of the relative concentration of CR as a function of time is shown in figure 5. The figure shows the photocatalytic activity of CPH-synthesized NCs along with that for the commercial TiO_2 , and for one SSR-

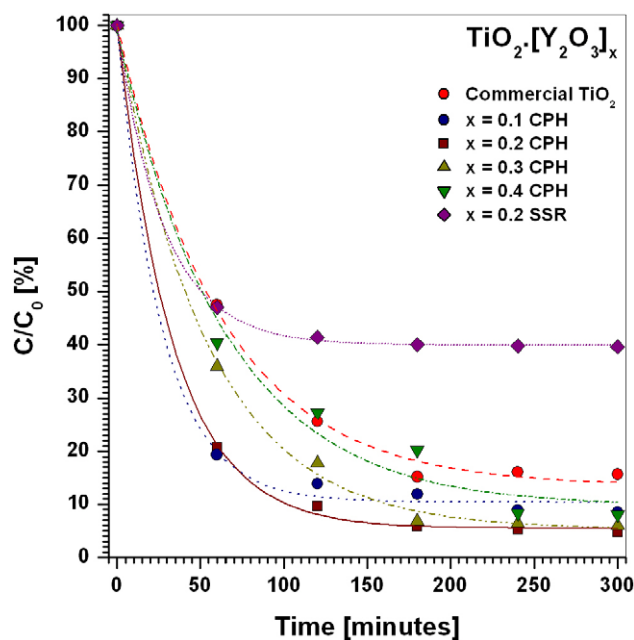


Figure 5. Photocatalytic degradation with time of congo red in the presence of $\text{TiO}_2 \cdot [\text{Y}_2\text{O}_3]_x$ NCs. The degradations with commercial TiO_2 and SSR-prepared $\text{TiO}_2 \cdot [\text{Y}_2\text{O}_3]_{0.2}$ are also shown for comparison.

prepared sample, for comparison. No obvious degradation of CR was observed either with the sample but in the absence of irradiation; or under light but without any photocatalyst. From these degradation results, the rate of degradation of CR was found to be of first order for all the catalysts. The apparent rate constant (k_{obs}) for the degradation process was estimated from a least-squares regression of $\ln(C/C_0)$ versus time.

Substantial degradation of CR was observed with all the CPH-synthesized NC samples. The $x = 0.1, 0.2, 0.3$ and 0.4 samples degraded about 91%, 95%, 92% and 86% of CR, respectively, after 180 min (table 1). The fastest initial degradation, however, was observed for the CPH-synthesized NC with $x = 0.1$ with a value of $k_{\text{obs}} = 2.74 \times 10^{-2} \text{ min}^{-1}$, which was only marginally higher than that for the $x = 0.2$ composition with $k_{\text{obs}} = 2.62 \times 10^{-2} \text{ min}^{-1}$. In contrast, the SSR-prepared samples showed much less degradation after the same time interval, with a maximum degradation of about 60% recorded with the $x = 0.2$ (with $k_{\text{obs}} = 1.20 \times 10^{-2} \text{ min}^{-1}$) polycrystalline sample. Even the commercial pure TiO_2 (predominantly rutile) showed better results of about 80% degradation of CR in 180 min, although at a slower initial rate of $k_{\text{obs}} = 1.07 \times 10^{-2} \text{ min}^{-1}$, in comparison with the SSR composites.

The above results of photocatalytic degradation of CR point to some interesting conclusions. As mentioned earlier, the role of bandgap modification in the observed photocatalytic activity of these composites is apparently negligible, at least in the present example with the degradation of CR. This inference is based on the fact that the bandgap is not favorably modified by Y_2O_3 doping of TiO_2 , because the former has a wider bandgap. Consequently, with doping

Table 1. Degradation of congo red in the presence of various TiO₂ based photocatalysts.

Particle	Crystallite size (nm)	Particle size	Rate of degradation of CR, k_{obs} ($\times 10^{-2} \text{ min}^{-1}$)	% CR degraded after 180 min
Commercial TiO ₂	57	2.44 μm	1.07	85
CPH TiO ₂ [Y ₂ O ₃] _{0.1}	16	74 nm	2.74	91
CPH TiO ₂ [Y ₂ O ₃] _{0.2}	19	75 nm	2.62	95
CPH TiO ₂ [Y ₂ O ₃] _{0.3}	16	75 nm	1.71	92
CPH TiO ₂ [Y ₂ O ₃] _{0.4}	16	73 nm	1.52	86
SSR TiO ₂ [Y ₂ O ₃] _{0.2}	41	2.34 μm	1.20	60

the value of λ_{cutoff} is expected to shrink back into the UV regions of the spectrum, instead of getting extended towards the higher wavelengths as required for visible light photocatalysis by photo-excitation. Essentially, therefore, the TiO₂·[Y₂O₃]_x mediated photocatalytic degradation of CR takes place through the process of photosensitization. In this process, the dye molecules get adsorbed to the catalyst surface, and start absorbing the incident radiation to get photochemically excited, which eventually leads to their degradation. Obviously, the available specific surface area of the catalyst plays a major role in this process, and thus the size of the particle becomes important, since for a given amount of material, the particles with smaller size contribute to larger specific surface area. This discussion leads to the possible explanation that the smaller particle size of the TiO₂·[Y₂O₃]_x NCs with an average value around 74 nm, is clearly the factor primarily responsible for better photocatalytic degradation of CR. The SSR-prepared samples showed lesser photocatalytic activity apparently because of their larger average particle size of about a few micrometers. In addition, the better degradation after 180 min showed by the commercial TiO₂ with respect to the SSR-prepared composites (mainly rutile), even though the two had comparable particle sizes, may be attributed to the decreased proportion of the active material in the latter. The faster degradation rate (k_{obs}) observed with the polycrystalline composites, however, clearly points out the role of Y³⁺ doping, which is discussed later.

At this point, it is noteworthy to mention that the improved photocatalytic activity of TiO₂·[Y₂O₃]_x composites does not seem to be directly associated with the TiO₂ phases (anatase and rutile), since the XRD results do not show any such transformations taking place at higher doping. Moreover, the specific dependence of the photocatalytic activity on the two TiO₂ phases is still not very clear, and several authors have reported that both the TiO₂ phases independently, or as a mixture, can support photocatalysis [13, 14, 32], although anatase is perhaps slightly more conducive than rutile in the photodegradation of CR [14]. In this view, while it might appear that the presence of the anatase phase is partly responsible for the better catalytic activity of CPH-synthesized NCs, we can safely ignore this dependence because the observations related to the particle size are believed to be much more pronounced.

Therefore, at first glance, the smaller particle size seems to be the only factor responsible for the enhanced photocatalytic activity of the TiO₂·[Y₂O₃]_x NCs. However, a comparison between these results and that already reported for the

pure TiO₂ nanoparticle-mediated photocatalytic degradation of CR [14] clearly points to the role of Y³⁺ doping in the enhanced activity. A rough estimation of the initial rate of degradation, k_{obs} , from the data reported by Wahi *et al* [14] yields approximate values of $0.07 \times 10^{-2} \text{ min}^{-1}$ and $0.05 \times 10^{-2} \text{ min}^{-1}$, respectively, for anatase TiO₂ nanodots of 15 and 10 nm (crystallite-) size, which were the two best performing catalysts in that work. In terms of the per cent degradation, the 15 nm particles apparently degraded about 70%, whereas the 10 nm particles degraded nearly 60% of CR after 180 min. It is thus evident that the Y³⁺-doped NCs (especially with $x = 0.1$ – 0.3), even with slightly bigger crystallite size of about 16–19 nm, lead to much better degradation of CR as compared to the pure TiO₂ nanodots. Interestingly, both estimated values of k_{obs} for TiO₂ nanodots are smaller than that for the SSR-prepared composite ($x = 0.2$) and for commercial TiO₂ of our work (see table 1). The first of these observations may be attributed to the effects of Y³⁺ doping as well, whereas the second, to the increased rate of e⁻/h⁺ recombination, which hinders the photocatalytic activity in smaller particles of the undoped material [14]. The latter inference is also supported by the fact that 15 nm nanodots appear to be a slightly better photocatalyst than the 10 nm nanodots, both in terms of estimated k_{obs} and per cent degradation. In brief, all the deductions from these comparisons could be summed up by stating that Y³⁺ doping improves the photocatalytic properties of the material through efficient reduction of e⁻/h⁺ recombination.

Another comparison of the results of the present investigation and those obtained earlier with Zn²⁺/Fe³⁺-doped TiO₂ NCs [13] further consolidates that Y³⁺ doping plays a significant role in the observed improvement of photocatalytic activity of the catalysts. Except for the type of doping, both Zn²⁺/Fe³⁺- and Y³⁺-doped NCs were prepared under similar conditions. In addition, they also contained the same phase of anatase TiO₂ [13] and therefore phase dependence, if any, is out of question in this comparison. In terms of the photocatalytic degradation of CR, Y³⁺ doping produces better photocatalysts than the Zn²⁺/Fe³⁺ doping. This is evident from two key observations. First, all the Y³⁺-doped NCs (for $x = 0.1$ – 0.4) showed significant photocatalytic activity of more than 85% degradation of CR after 180 min, whereas, with the Zn²⁺/Fe³⁺ doping, such a high activity was shown only by $x = 0.1$ and 0.2 samples. Second, the estimated rate constants for the Y³⁺-doped NCs (e.g. $k_{\text{obs}} = 2.74 \times 10^{-2} \text{ min}^{-1}$ for $x = 0.1$ doping) also are much higher than those of the similar Zn²⁺/Fe³⁺-doped compositions (e.g. $k_{\text{obs}} = 1.60 \times 10^{-2} \text{ min}^{-1}$

for $x = 0.1$ doping). Apart from these observations, a careful analysis just in terms of the particle sizes of the two best performing NCs from both sets also seems to support that the Y^{3+} doping is indeed responsible for some additional photocatalytic activity. The 71 nm (average size) particle of the Zn^{2+}/Fe^{3+} -doped composite ($x = 0.1$) showed 90% (with the rate $k_{obs} = 1.60 \times 10^{-2} \text{ min}^{-1}$) degradation after 180 min, whereas the Y^{3+} -doped composite ($x = 0.2$) with a marginally bigger size of 75 nm produced 95% ($k_{obs} = 2.62 \times 10^{-2} \text{ min}^{-1}$) degradation in the same time interval. Even the $x = 0.1$ Y^{3+} -doped sample with 74 nm average particle size showed 91% degradation with a faster rate of $k_{obs} = 2.74 \times 10^{-2} \text{ min}^{-1}$. If particle size was the sole reason for better performance of the NCs, it should have been the opposite trend both in terms of per cent degradation and the apparent rate constants!

From the above discussions it is evident that the presence of Y^{3+} ions essentially increases the rate of degradation of CR with the composites, irrespective of their different methods of preparation (i.e. effectively their size). However, when combined with the effects of smaller particle size, e.g. as in the case of NCs, it leads to an overall improvement of photocatalytic activity. It should be remembered that the dopant Y_2O_3 is practically inactive under visible light because of its bandgap of about 4.5 eV ($\lambda_{cutoff} = 275 \text{ nm}$) [23], which corresponds to UV-C (or 280–100 nm) irradiation to initiate photocatalysis [33]. Or, in other words, Y_2O_3 is not directly involved in the visible light photocatalytic degradation of CR. Nevertheless, the presence of rare earth ions is expected to suppress the unwanted e^-/h^+ recombination via trapping of the electrons [24–26] produced from the photochemically excited dye molecules adsorbed on the TiO_2 surface. Therefore, it seems plausible that the Y^{3+} ions additionally contribute to the degradation of CR by efficiently controlling the e^-/h^+ recombination, which otherwise severely hampers the photocatalytic activity of the materials.

4. Conclusions

The visible light photocatalytic behavior of $TiO_2 \cdot [Y_2O_3]_x$ nanocomposites synthesized chemically by the co-precipitation/hydrolysis method has been investigated through the degradation of the dye congo red. It was observed that all compositions ($x = 0.1$ – 0.4) of the nanocomposites investigated lead to very efficient degradation of the dye, both in terms of the percentage degradation after 180 min, as well as the apparent rate constants. When these results were compared to those obtained with solid-state reaction-prepared samples of similar compositions, the role of smaller particle size became evident. Hence, it was concluded that photosensitization was the process responsible for the photodegradation of congo red in the presence of these materials. Further, a comparison between the results obtained with Y^{3+} -doped TiO_2 nanocomposites, pure TiO_2 nanodots and Zn^{2+}/Fe^{3+} -doped nanocomposites in the degradation of the same dye revealed that Y^{3+} doping was responsible for the marked improvement of photocatalytic properties. The effective inhibition of the e^-/h^+ recombination due to the presence of Y^{3+} ions is the possible reason for this observed improvement.

The results of this investigation look extremely promising because the photocatalysts used are expected to be effective in the degradation of practically any dye. Since congo red absorbs towards the higher wavelength regions of the visible spectrum, most of the other dyes that absorb lower (e.g. indigo blue) to medium (e.g. methyl orange) wavelengths are likely to be degraded by means of photosensitization using these, or similar, catalysts. This is because the process of photosensitization mainly depends upon the wavelengths of light absorbed by the dye, and not on the wavelengths absorbed by the catalysts. More work is in progress.

References

- [1] Linsebigler A L, Lu G and Yates J T 1995 *Chem. Rev.* **95** 735–58
- [2] Kazuhito H 2005 *Japan. J. Appl. Phys.* **2** **44** 8269–85
- [3] Bumpas J A, Tricker J, Andrzejewski K, Rhoads H and Tatarko M 1999 *J. Chem. Educ.* **76** 1680–3
- [4] Uyguner C S and Bekbolet M 2007 *Int. J. Photoenergy* **2007** 23156
- [5] Vogel R, Pohl K and Weller H 1990 *Chem. Phys. Lett.* **174** 241–6
- [6] Liu D and Kamat P V 1993 *J. Phys. Chem.* **97** 10769–73
- [7] Ennaoui A, Fiechter S, Tributsch H, Giersig M, Vogel R and Well H 1992 *J. Electrochem. Soc.* **139** 2514–8
- [8] Ashokkumar M, Kudo A, Saito N and Sakata T 1994 *Chem. Phys. Lett.* **229** 383–8
- [9] Do Y R, Lee W, Dwight K and Wold A 1994 *J. Solid State Chem.* **108** 198–201
- [10] Li X Z, Li F B, Yang C L and Ge W K 2001 *J. Photochem. Photobiol. A* **141** 209–17
- [11] Srinivasan S S, Wade J and Stefanakos E K 2006 *J. Nanomater.* **2006** 45712
- [12] Yuan Z-H and Zhang L-d 2001 *J. Mater. Chem.* **11** 1265–8
- [13] Narayan H, Alemu H M, Macheli L, Sekota M, Thakurdesai M and Gundu Rao T K 2009 *Bull. Mater. Sci.* at press
- [14] Wahi R K, Yu W W, Liu Y, Mejia M L, Falkner J C, Nolte W and Colvin V L 2005 *J. Mol. Catal. A* **242** 48–56
- [15] Khan M A, Jung H-T and Yang O-B 2006 *J. Phys. Chem. B* **110** 6626–30
- [16] Dung N T, Khoa N V and Herrmann J M 2005 *Int. J. Photoenergy* **07** 11–5
- [17] Habibi M H, Esfahani M N and Egerton T A 2007 *Int. J. Photoenergy* **2007** 13653
- [18] Cheng P, Li W, Zhou T, Jin Y and Gu M 2004 *J. Photochem. Photobiol. A* **168** 97–101
- [19] Ward M D and Bard A J 1982 *J. Phys. Chem.* **86** 3599–605
- [20] Elizabeth C B and Allen P D 1993 *J. Photochem. Photobiol. A* **70** 273–83
- [21] Wei T-Y, Wang Y-Y and Wan C-C 1990 *J. Photochem. Photobiol. A* **55** 115–26
- [22] Satoh N, Nakashima T, Kamikura K and Yamamoto K 2008 *Nat. Nanotechnol.* **3** 106–11
- [23] Xu Y-N, Gu Z-q and Ching W Y 1997 *Phys. Rev. B* **56** 14993–5000
- [24] Liu J, Yang R and Li S 2007 *J. Rare Earths* **25** 173–8
- [25] Xie Y and Yuan C 2004 *Mater. Res. Bull.* **39** 533–43
- [26] Guan K-s and Yin Y-s 2005 *Mater. Chem. Phys.* **92** 10–5
- [27] Boulc'h F, Schouler M-C, Donnadieu P, Chaix J-M and Djurado E 2001 *Image Anal. Stereol.* **20** 157–61
- [28] Calvin S, Riedel C J, Carpenter E E, Morrison S A, Stroud R M and Harris V G 2005 *Phys. Scr. T* **115** 744–8
- [29] Dinnebier R E and Billinge S J L (ed) 2008 *Powder Diffraction: Theory and Practice* (Cambridge: Royal Society of Chemistry) chapter 5 p 142

- [30] Zhang W F, He Y L, Zhang M S, Yin Z and Chen Q 2000 *J. Phys. D: Appl. Phys.* **33** 912–6
- [31] Fonzo F D, Casari C S, Russo V, Brunella M F, Bassi A L and Bottani C E 2009 *Nanotechnology* **20** 015604
- [32] Liu G-g, Zhang X-z, Xu Y-j, Niu X-s, Zheng L-q and Ding X-j 2004 *Chemosphere* **55** 1287–91
- [33] Karunakaran C, Dhanalakshmi R and Anilkumar P 2009 *Radiat. Phys. Chem.* **78** 173–6